Reduced Retina Microglial Activation and Improved Optic Nerve Integrity with Minocycline Treatment in the DBA/2J Mouse Model of Glaucoma

Alejandra Bosco,[1,2,3] *Denise M. Inman,*[3,4] *Michael R. Steele,*[1,2] *Guangming Wu,*[5] *Ileana Soto,*[6,7] *Nicholas Marsh-Armstrong,*[6] *Walter C. Hubbard,*[8] *David J. Calkins,*[5] *Philip J. Horner,*[4] *and Monica L. Vetter*[1,2]

Purpose. In the context of the retinal ganglion cell (RGC) axon degeneration in the optic nerve that occurs in glaucoma, microglia become activated, then phagocytic, and redistribute in the optic nerve head. The authors investigated the potential contribution of retinal microglia activation to glaucoma progression in the DBA/2J chronic mouse glaucoma model.

Methods. The authors treated 6-week-old DBA/2J mice for 25 weeks with minocycline, a tetracycline derivative known to reduce microglia activation and to improve neuronal survival in other models of neurodegenerative disease. They quantified RGC numbers and characterized microglia activation, gliosis, and both axonal integrity and retrograde tracer transport by RGCs in mice systemically treated with minocycline or vehicle only.

Results. Minocycline reduced microglial activation and improved RGC axonal transport and integrity, yet it had no effect on the characteristic age-related ocular changes that lead to chronically elevated pressure and did not alter Müller or astrocyte gliosis. Specifically, minocycline increased the fraction of microglia with resting ramified morphology and reduced levels of Iba1 mRNA and protein, a microglia-specific calcium ligand linked to activation. The reduction in microglial activation was coupled to significant improvement in RGC axonal transport, as measured by neuronal retrograde tracing from the superior colliculus. Finally, minocycline treatment significantly decoupled RGC axon loss from increased intraocular pressure.

Conclusions. These observations suggest that in glaucoma, retina and optic nerve head microglia activation may be a factor in the early decline in function of the optic nerve and its subsequent degeneration. (*Invest Ophthalmol Vis Sci.* 2008; 49:1437–1446) DOI:10.1167/iovs.07-1337

Glaucoma progression toward chronic optic nerve atrophy and asynchronous death of retinal ganglion cells (RGCs) has two primary risk factors: age and high intraocular pressure (IOP).[1] Lowering IOP decelerates, but does not halt, glaucoma, suggesting that therapies targeting the pathogenesis of neurodegeneration might be a more promising approach for intervention. Glaucoma involves gliosis and innate immune responses,[1–57] suggesting a pathogenic function for microglia, which are the resident immune surveillance cells in the central nervous system and retina.

In the adult, microglia are quiescent unless pathogens, injury, or stress trigger their proliferation, migration, and activation. Within the healthy adult retina, perivascular and parenchymal "resting" microglia localize to the inner retina,[6] becoming activated and migratory after RGC axotomy,[7] ischemia,[8] photoreceptor degeneration,[9] and endothelin-induced optic neuropathy.[10] In persons with glaucoma, microglia become activated and redistributed within the optic nerve head (ONH),[11,12] producing proinflammatory cytokines, reactive oxygen species, neurotoxic matrix metalloproteinases, and neurotrophic factors. Activated microglia produce cytokines/chemokines or cytotoxins and have phagocytic activity,[13,14] but the specific influence of microglial factors on other retinal cells, including RGCs, is unclear, though potentially linked to glaucoma pathology.[6,15]

Minocycline, a neuroprotective tetracycline derivative that suppresses chronic neuroinflammation and microglial activation,[16] protects RGCs after axotomy[17,18] and in optic neuritis models.[19] We questioned whether retinal microglia deactivation during early glaucoma progression might protect the optic nerve from degeneration. The effects of systemic, long-term administration of minocycline on optic neuropathy and retinal microglia were studied in DBA/2J mice. This model of secondary glaucoma replicates key aspects of the human pathology, including IOP increase caused by blockage of the anterior drainage pathways of the eye, IOP-dependent loss of RGC axons, gliosis, and microglia proliferation in the vicinity of RGCs.[20–23] We demonstrate that the reduction of retinal microglia activation reverses the typical loss of RGC axonal transport and integrity that normally accompanies IOP elevation (Inman DM, et al. *IOVS* 2007;48:ARVO E-Abstract 3291).

Materials and Methods

Mice

DBA/2J mice originally obtained from Jackson Laboratories (Bar Harbor, ME) were bred and housed in a pathogen-free barrier facility at the

From the Departments of [1]Neurobiology and [2]Anatomy, University of Utah, Salt Lake City, Utah; [4]Department of Neurosurgery, University of Washington, Seattle, Washington; [5]Department of Ophthalmology and Visual Sciences, Vanderbilt University, Nashville, Tennessee; [6]Kennedy Krieger Institute, Baltimore, Maryland; and [7]Solomon Snyder Department of Neuroscience and [8]Division of Clinical Pharmacology, Johns Hopkins School of Medicine, Baltimore, Maryland.

[3]These authors contributed equally to the work presented here and should therefore be regarded as equivalent authors.

Supported by Catalyst for a Cure funding from the Glaucoma Research Foundation (MLV, DJC, PJH, NM-A) and the mass spectrophotometer by National Institutes of Health Grant 1S10 RR16798 (WCH).

Submitted for publication October 17, 2007; revised December 12, 2007; accepted February 18, 2008.

Disclosure: **A. Bosco**, None; **D.M. Inman**, None; **M.R. Steele**, None; **G. Wu**, None; **I. Soto**, None; **N. Marsh-Armstrong**, None; **W.C. Hubbard**, None; **D.J. Calkins**, None; **P.J. Horner**, None; **M.L. Vetter**, None

The publication costs of this article were defrayed in part by page charge payment. This article must therefore be marked "*advertisement*" in accordance with 18 U.S.C. §1734 solely to indicate this fact.

Corresponding author: Alejandra Bosco, Departments of Neurobiology and Anatomy, University of Utah, 517 Wintrobe, 20 North 1900 East, Salt Lake City, UT 84132; alebosco@neuro.utah.edu.

University of Washington Harborview Medical Center (Seattle, WA). Mice were maintained in a 12-hour light/12-hour dark cycle and fed ad libitum. Experiments and animal care procedures adhered to the ARVO Statement for the Use of Animals in Ophthalmic and Vision Research and to the guidelines of the University of Washington Institutional Animal Care and Use Committee.

IOP Measurement

IOP was measured (Tono-Pen XL; Medtronic Solan, Jacksonville, FL) as previously described.[21] During each session (Fig. 1A), 20 measurements were averaged per eye. Here we report the actual IOP at each age (IOP), the last IOP measurement before kill (final IOP), or the average IOP across the life of the mouse (mean IOP ± SD).

Minocycline Administration

Experimental mice ($n = 25$) at 6 weeks of age received intraperitoneal minocycline hydrochloride (Sigma-Aldrich, St. Louis, MO; 120 mg/kg[24]) until they were large enough for gavage (3 weeks). For the next 22 weeks, minocycline was delivered daily by gavage with a dose not exceeding 1% wt/vol[25] using a blunt nonstick (Teflon)-tipped 20-gauge needle (Popper and Sons, New Hyde Park, NY). Vehicle mice ($n = 25$) received 5% sucrose in 0.9% saline solution by identical routes. Gavage guaranteed controlled dosing and eliminated injection scarring (timeline schematized in Fig. 1A).

RGC Retrograde Labeling

At dosing week 24, bilateral holes were drilled into the craniums (−4.0 bregma, ±0.5 midline) of a subset of mice (8 in the vehicle group, 7 in the minocycline group) under 2,2-tribromoethanol (1.3%) and tert-amyl alcohol (0.8%) in dH_2O (Sigma-Aldrich) anesthesia in a stereotaxic device (David Kopf Instruments, Tujunga, CA). The superior colliculi (0.5 mm below dura) were injected with 2 μL of 1% neuronal retrograde tracer (Fluoro-Gold; Molecular Probes, Eugene, OR) in hydroxystilbamidine (dH_2O) over 2 minutes, and holes were filled with sterile compressed sponge (Gelfoam; Pfizer, New York, NY) soaked in 5% neuronal retrograde tracer. Scalps were sutured with 4-0 silk.

Tissue Collection

Seven-month-old mice were perfused with 4% paraformaldehyde in 0.1 M phosphate buffer (PB), pH 7.4; brains, optic nerves, and eyes were removed, postfixed for 1 hour, and stored in PB until processing. The superior quadrant was marked in situ on all globes.

Minocycline Mass Spectrometry

After 2 weeks of intraperitoneal minocycline, retinas ($n = 6$) and brains ($n = 3$) from saline-perfused mice were frozen in liquid N_2 and homogenized in ice-cold PB saline (5 mL/g). The internal standard (0.15 μg tetracycline) and H_3PO_4 (20 μL) were added to 1 mL homogenate and centrifuged (2000 rpm for 30 minutes at 4°C). The redissolved supernatants were combined and cleaned up with 1 mL/30 g extraction cartridges (Oasis HLB; Waters, Mildford, MA). Samples were eluted with 1 mL methanol and evaporated under a nitrogen stream (40°C), and the residue was dissolved in 200 μL and measured in a mass spectrometer (PE Sciex API4000; Applied Biosystems, Foster City, CA) coupled with a liquid chromatograph (model 1100; Agilent Technologies, Wilmington, DE). Chromatographic resolution used a 50 × 4.6-mm column, 5-μm particle size (Zorbax Eclipse XDB MS C8; Agilent Technologies), with 5% formic acid/0.5% formic acid methanol gradient. For identification, multiple reaction monitoring (MRM) transitions usedm/z 458 > 441 and 458 > 352 for minocycline and m/z 445 > 410 and m/z 445 > 427 for tetracycline. The signal at the MRM transitions at m/z 458 > 441 and 445 > 427 was used to quantify minocycline levels. Parameters were optimized for declustering potentials, collision energies, and ext potentials. Values are expressed per tissue and are not based on tetracycline, avoiding the inaccuracy of wet

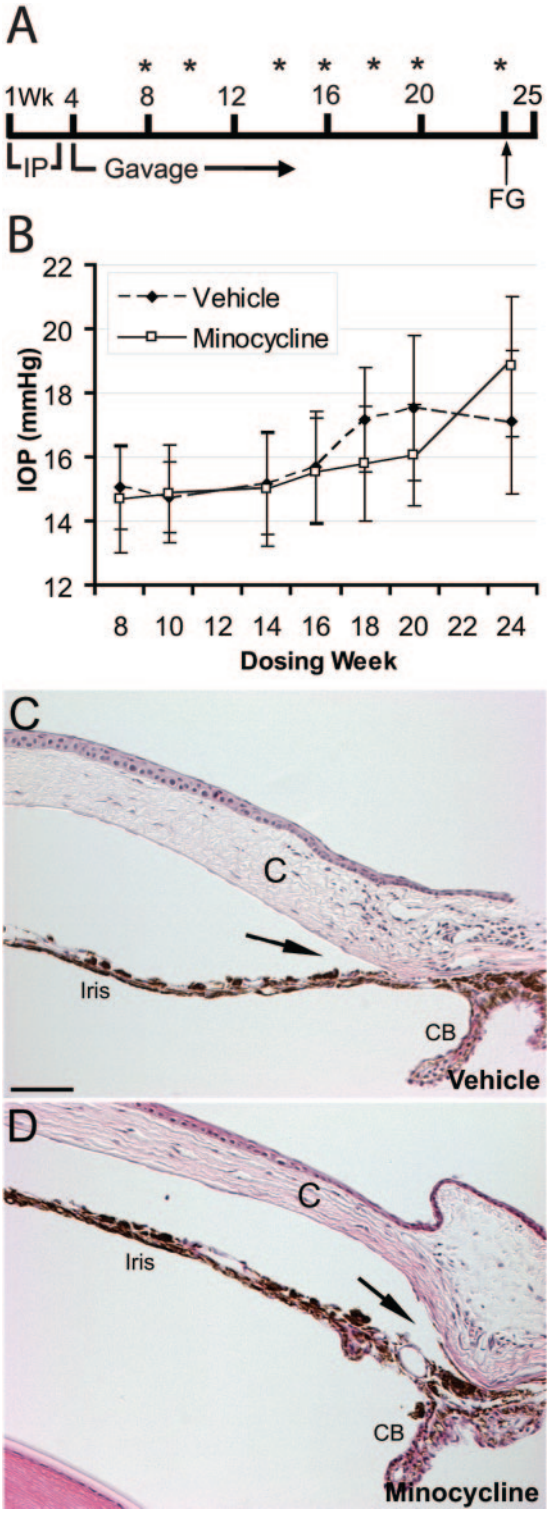

FIGURE 1. Experimental timeline. (**A**) Six-week-old mice were started on minocycline (120 mg/kg) or vehicle dosing first by intraperitoneal injection (3 weeks), then by oral gavage (dosing weeks 4–25); IOP was periodically measured (*asterisks*). Minocycline tissue levels were assayed after 2 weeks of dosing. RGCs were retrolabeled at dosing week 24. Tissue was harvested for histopathology, immunofluorescence, and qRT-PCR at dosing week 25 (7 months of age). (**B**) IOP measurements show no significant differences between vehicle and minocycline groups, except at dosing week 18 ($P < 0.05$). Error bars = SD. (**C**, **D**) Cross-sections of the corneal limbus showing iris, cornea (C), and ciliary body (CB) and comparable closure of the iridocorneal angles (*arrow*) in vehicle (**C**) and minocycline (**D**) groups. Scale bar, 500 μm.

weight values. For brain data, raw values and those relative to tetracycline were nearly identical.

Immunolabeling

Retinas dissected in PB saline were processed and immunolabeled as previously described for cryosections[26] and flatmount preparations.[20] Primary antibodies included GFAP (1:1000; Advanced Immunochemicals), Iba1 (1:300; Wako Chemicals, Inc., Tokyo, Japan), cleaved caspase 3 (1:50; Cell Signaling, Danvers, MA), and NeuN (1:500; Chemicon, Temecula, CA). Secondary antibodies conjugated to diverse fluorophores (Jackson ImmunoResearch Laboratories, Inc., West Grove, PA) were used for single to triple immunolabeling, showing no specific binding to the tissue after primary antibody omission. Serial sections were stained with hematoxylin-eosin for histologic analysis of the eye anterior segment.

Stereology and Axon Counts

Numbers of NeuN-positive and neuronal retrograde tracer-positive RGCs, GFAP-positive astrocytes, and Iba1-positive microglia in flatmount retinas were estimated by unbiased stereological analysis (StereoInvestigator; MicroBrightfield, Middlebury, VT). Cells were counted, at 20× magnification, throughout 2.14% to 3.42% of the retinal surface (40 sampling sites), at all focal planes. Central quadrants were traced as a circle (radius, 1500 μm) centered on the ONH, and the peripheral quadrants were traced along the retinal periphery. Total cell density was determined by summing the total areas for each sampling sector and dividing by the summed value of the stereological estimate of the cell population for all sectors. Cell numbers were also quantified by retinal quadrant and eccentricity.

Counts of RGC axons in 1- to 2-mm lengths of optic nerve proximal to the posterior eyecup were obtained as previously described.[21] The cross-sectional area of every axon counted was quantified as the axoplasm area contained within the best-fitting polygon around the axon perimeter defined by the myelin sheath (ImagePro; Media Cybernetics, Bethesda, MD).

Morphometry and Densitometry

Microglial cell ramification was calculated for all cells within 60× microscope fields spaced 500 μm along the superior-inferior and nasal-temporal retinal axes beginning at the ONH (Fig. 2A). Cells localized from the outer plexiform layer (OPL) to the ganglion cell layer (GCL). Primary processes and process tips were counted for each cell; ramification is the number of tips divided by number of primary processes (Fig. 2A). There were 3 to 15 cells per microscope field, 20 fields per retina, and 6 retinas for each group. Those retinas in which microglia ramification was measured also had their RGCs retrogradely labeled with neuronal retrograde tracer, which allowed us to correlate levels of microglia activation and numbers of neuronal retrograde tracer-positive RGCs.

To measure microglial solidity, sagittal retinal sections spanning the ONH (two retinas from different individuals per group) were examined at 200× and imaged as 10 μm-deep stacks (every 0.5 μm) with an laser confocal microscope (Fluoview; Olympus, Tokyo, Japan), sampling at least 15 × 125-μm^2 areas, maintaining identical settings and eccentricity. For each microglial soma (at least 15 cells per quadrant), a cell silhouette was hand traced, and a polygon was drawn enclosing the entire cell; then the cell and the polygon area and perimeter were measured. Solidity was calculated as the ratio of cell area over polygon area.[29] In the same retinal sections, the relative intensity of Iba1 immunofluorescence within the defined cell area (10 cells per quadrant) was quantified and reported as mean values (range, 0–4095 AU; Fluoview 4.3; Olympus); focus coincided with the highest pixel intensity at the soma center.

Another set of retinal sections (two retinas from different individuals per group) was examined at 100× and imaged as 20 μm-deep stacks (every 1.5 μm) to measure GFAP-immunofluorescence relative intensity in each optical slice along lines transecting the GCL, inner nuclear layer (INL), inner plexiform layer (IPL), and OPL, from the superior to the inferior retinal margins. Identical x-y positions were averaged across the stack and analyzed by eccentricity. Data presented are means for the line scan crossing each layer.

qRT-PCR

Total RNA was extracted from 7-month-old mouse retinas ($n = 6$ per group) using published methods.[6] Real-time PCR reactions were completed using the following primer sets: Iba1, 5′-CCTGATTGGAGGTGGATGTCAC-3′ and 5′-GGCTCACGACTGTTTCTTTTTTCC-3′; GFAP, 5′-CCGTTCTCTGGAAGACACTGAAAC-3 and 5′-TTGGAAGGATGGTTGTGGATTC-3′; β-actin, 5′-TGAGAGGGAAATCGTGCGTG-3′ and 5′-TCGTTGCCAATAGTGATGAC CTG-3′. Changes in gene expression levels were determined relative to β-actin, a reference that did not change significantly in our samples.

Statistical Analysis

Data are presented as mean and error bars as SEM, except for IOP measurements, which are presented as SD. Analysis of variance was performed for IOP comparisons, with a Dunn post hoc multiple comparison test. Student's *t*-test was performed for comparisons of cell numbers, ramification, protein, and mRNA expression.

Results

Unchanged Anterior Segment Pathology and IOP Elevation

To determine whether the inhibition of retinal microglia activation in DBA/2J mice during the onset of glaucoma would affect its progression, we investigated whether long-term minocycline administration could suppress retinal microglia activation and rescue RGC axonopathy. Minocycline, a semisynthetic derivative of tetracycline, readily crosses the blood-brain barrier.[27] Starting at 6 weeks of age, before the onset of retinal pathology in DBA/2J mice, minocycline ($n = 25$) or vehicle ($n = 25$) was administered intraperitoneally for 3 weeks and then administered by oral gavage for 22 weeks (Fig. 1A). As determined by liquid chromatography–tandem mass spectrometry, the tissue levels of minocycline after 2 weeks of intraperitoneal delivery were 0.44 ± 0.2 μg/brain ($n = 3$) and 0.29 μg/retina ($n = 6$), values that exceed efficacy levels for minocycline.[24] Although the DBA/2J strain is prone to audiogenic seizure,[28] the occasional seizure was observed in the minocycline group only, suggesting that its long-term administration contributed to the seizure incidence.

DBA/2J mouse IOP increases from 3 to 9 months of age as a result of aqueous humor drainage block from iris stromal atrophy and pigment dispersion.[29,30] Here, long-term minocycline treatment did not alter the anterior segment pathology at 7 months of age because vehicle- and minocycline-treated mice showed similar degrees of iris pigment dispersion and iridocorneal angle closure (Figs. 1C, 1D). Periodic applanation tonometer (Tono-Pen; Reichert, Depew, NY) measurements during treatment (Fig. 1A) revealed no IOP differences in vehicle- and minocycline-treated mice except at 18 weeks of dosing, when the IOP variance was significantly different between the groups (Fig. 1B; $P < 0.05$). At 20 and 24 weeks of dosing, IOP converged to similar levels in both groups and was comparably elevated in both groups at 24 weeks (Fig. 1B). At each age, the average IOP of both groups was comparable to that of previously published values for DBA/2J mice.[21] Together, these results indicated that minocycline did not alter the course of anterior segment disease and the concomitant IOP elevation.

Retinal Gliosis Unaffected

We reported previously that the DBA/2J retina initiates astrocyte and Müller cell nonproliferative reactive gliosis beginning

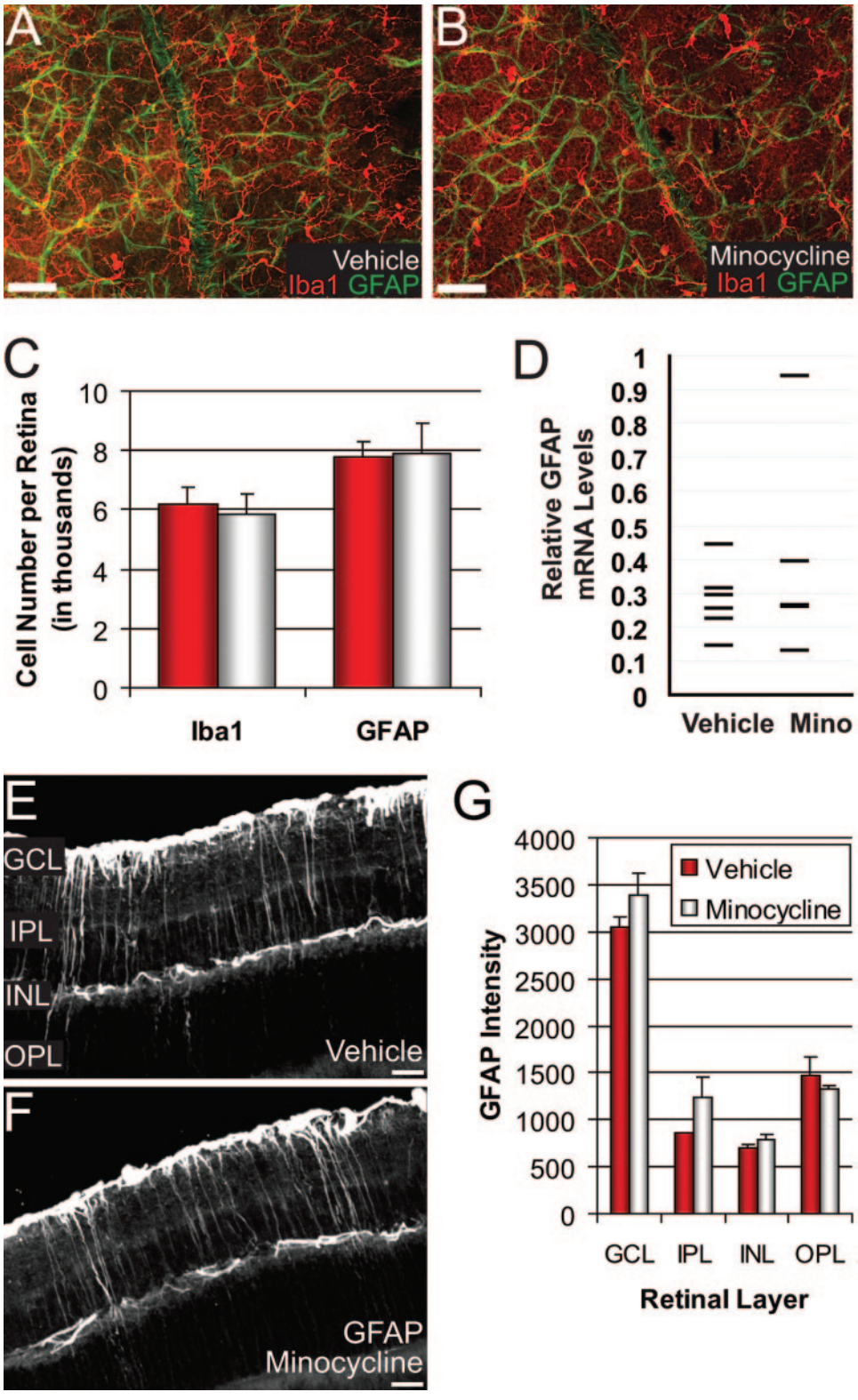

FIGURE 2. (**A**, **B**) Retinal flatmounts showing Iba1-positive microglia (*red*) distributed throughout the inner retina and among GFAP-positive astrocyte (*green*) somata and processes in 7-month-old mice treated with vehicle (**A**) or minocycline (**B**). Scale bars, 25 μm. (**C**) Quantitative stereological estimation of the numbers of Iba1-positive microglia and GFAP-positive astrocytes throughout all retinal layers confirmed no differences between vehicle (*dark bars*, $n = 8$) and minocycline (*light bars*, $n = 7$) groups. (**D**) qRT-PCR assay of GFAP mRNA levels in vehicle- and minocycline-treated retinas detected no significant differences in average mRNA levels (vehicle, 0.28 ± 0.04; minocycline, 0.40 ± 0.14), though the graph depicts the range of values for individual retinas ($n = 6$ per group). (**E**, **F**) Retinal sections immunolabeled with GFAP (astrocytes and Müller glia) in 7-month-old vehicle- (**E**) and minocycline-treated mice (**F**) revealed similar levels of expression across the retina. (**G**) Quantification of GFAP immunofluorescence relative intensity in retinal sections, across the GCL, IPL, OPL, and INL, confirmed the lack of significant differences in GFAP intensity between treatments. Scale bars, 25 μm.

at 3 months of age, whereas microglia numbers double between 4 and 10 months of age.[20] Retinas from 7-month-old vehicle- and minocycline-treated mice were double-immunolabeled for astrocytic GFAP (glial fibrillary acidic protein) and microglial Iba1, a retinal microglia-specific[20] (Figs. 2A, 2B) calcium-binding adaptor protein.[31] Stereological cell counts revealed no difference in numbers of GFAP-positive astrocytes and Iba1-positive microglia in vehicle compared with minocycline retinas (Fig. 2C). Moreover, peripheral and central regions showed no significant differences in microglia number or distribution between treatment groups (data not shown).

To further determine whether minocycline affected retinal gliosis, as measured by GFAP levels in astrocytes and Müller cells, we performed qRT-PCR analysis of GFAP mRNA relative to β-actin in 7-month-old retinas ($n = 6$ per treatment). Figure 2D demonstrates that most retinas expressed comparable lev-

els of GFAP, regardless of treatment group. Similarly, immunofluorescence analysis showed comparable GFAP protein expression in both groups (Figs. 2E, 2F). Densitometry of GFAP immunofluorescence on sagittal retinal sections revealed similar relative intensities and distributions of GFAP expression in retinas from both treatment groups, across cell compartments corresponding to astrocytes and Müller cell end feet (Fig. 2G), at the level of the GCL and processes, and across the plexiform layers. Only the IPL within the inferior quadrant had higher GFAP levels in retinas of minocycline-treated animals compared with the vehicle-treated group (data not shown).

Reduced Retinal Microglial Activation

Activated microglia observed in human glaucomatous ONH suggest a link between microgliosis and axonopathy.[32] With the knowledge that minocycline did not affect microglial cell number, we investigated whether minocycline reduced retinal microglial activation by using cell morphology as a readout for changes in the continuum between ramified/resting and solid/activated states (Fig. 3D). In different retinal preparations from 7-month-old mice, we measured cell ramification and solidity. Microglia ramification was assessed in flatmounted retinas immunolabeled for Iba1, at all depths and along each quadrant (Figs. 3A, 3B). Microglial cells were consistently more ramified (resting) in the minocycline group than in vehicle-treated retinas, suggesting a reduction in their activation state (Fig. 3E). Furthermore, microglia located at midperipheral eccentricity (1000 μm from the ONH) showed significantly higher ramification in minocycline-treated mice ($P < 0.05$).

Iba1, which is involved in membrane ruffling through actin-bundling activity[33,34] and through cell migration and phagocytosis,[35] is upregulated in activated microglia. Thus, to further monitor microglial activation, we quantified the levels of Iba1 mRNA and protein in retinas after 25 weeks of minocycline or vehicle treatment. As assessed by qRT-PCR, whole retina Iba1 mRNA in minocycline-treated mice ($n = 6$ per treatment) was approximately 38% lower on average than in vehicle-treated mice (data not shown). The quantification of Iba1 protein expression by densitometry of immunofluorescence intensity in individual microglial cells (317 cells from two different retinas per treatment) revealed a significant reduction (43%) in Iba1 levels in cells from minocycline-treated retinas compared with the vehicle-treated group (Fig. 3F; $P < 0.001$). Finally, we generated histograms of Iba1 fluorescence intensity and microglial cell solidity, comparing vehicle- and minocycline-treated retinas. We found that cells of similar morphologic complexity (e.g., solidity[29]) had significantly lower Iba1 intensity values if derived from minocycline-treated retinas than from vehicle-treated microglia (Fig. 3G), further confirming the selective decline of microglial activation by minocycline.

Improved RGC Viability

RGC axonal retrograde transport and connectivity to the superior colliculi declines with age and IOP and serves as an early indicator of RGC pathology in the DBA/2J retina well before the onset of RGC death (Buckingham BP, et al. *IOVS* 2006 47:ARVO E-Abstract 1237).[58] Thus, after having established that minocycline decreased microglia activation while leaving gliosis and anterior segment pathology unaltered, we determined whether minocycline treatment resulted in improved RGC axonal integrity. RGC somata were retrogradely labeled by bilateral injection of neuronal retrograde tracer in the superior colliculi. One week later, at dosing week 25, retinas from these mice were immunostained for NeuN, which strongly labeled all RGCs while it only weakly labeled displaced amacrine cells, which were excluded from this analysis. Healthy RGCs with normal axonal transport and functional projections to their target strata in the superior colliculi were double-labeled with neuronal retrograde tracer and NeuN, whereas those RGCs lacking normal connectivity or transport stained only for NeuN (Figs. 4A, 4B). Stereology counts of both populations of RGCs provide a measure of relative RGC axonal connectivity (Buckingham BP, et al. *IOVS* 2006 47:ARVO E-Abstract 1237).[36–38] Total NeuN-positive RGC numbers did not vary between vehicle (49,656 ± 421 cells) and minocycline (48,914 ± 2838 cells) groups, but minocycline-treated mice had significantly ($P < 0.05$) more neuronal retrograde tracer-positive RGCs than vehicle-treated mice (47,990 ± 2924 vs. 39,552 ± 5461; Fig. 4C). This difference indicated that minocycline selectively protected the retrograde transport of neuronal retrograde tracer to RGC somata, suggesting improved axonal connectivity. Further supporting the beneficial effect of reducing microglia activation on RGC axon transport, Figure 4E illustrates the enhanced correlation between numbers of neuronal retrograde tracer-positive RGCs and microglia ramification detectable in the retinal midperiphery (1000 μm from ONH) after minocycline treatment. In this scatter plot, microglia ramification is highly correlated to neuronal retrograde tracer-positive RGC number for the minocycline treatment group ($r^2 = 0.73$), suggesting that reduced microglial activation is associated with healthier RGCs. Although ramification is less correlated to neuronal retrograde tracer-positive RGC number for the vehicle treatment ($r^2 = 0.39$), ramification is a good predictor of neuronal retrograde tracer-positive RGCs overall.

Additionally, given that minocycline can inhibit caspase-3–dependent pathways of neuronal death[39] and that RGC apoptosis can be detected in 6-month-old DBA/2J retinas,[40] we examined whether minocycline had a direct effect on RGC apoptosis. Retinal sections immunolabeled for cleaved caspase-3 and NeuN showed no observable differences in the number of NeuN-positive activated caspase-3–positive RGCs between vehicle- and minocycline-treated retinas (data not shown).

Increased Optic Axon Survival and Caliber

As IOP increases in the aging DBA/2J retina, RGC axons are lost in the optic nerve proximal to the eye.[22] Our own work demonstrates that even subtle differences in IOP can lead to substantial differences in the number of surviving axons in comparably aged animals.[21] Thus, we sought to determine whether minocycline alters this IOP-dependent axonal degeneration by examining semithin cross-sections of optic nerve. An example of a vehicle group nerve demonstrates the usual pathology associated with elevated IOP in the DBA/2J retina, including disjointed myelin sheaths, thinning of axon density, and disorder within individual fascicles of axons (Fig. 5A). These features were far less prominent in a nerve from a minocycline-treated animal (Fig. 5B). To test these differences, we used digital light microscopy to quantify axon number and size in subsets of mice ($n = 6$ per group), as described.[21] Importantly, mean IOP (±SD) did not differ among these mice (Fig. 5D).

Foremost, RGC axons in minocycline-treated nerves (Fig. 5B) appeared to have a greater cross-sectional area than their vehicle-treated counterparts (Fig. 5A); this difference was not uniform across all axons. Rather, when quantified, minocycline increased the fraction of axons of medium caliber size only (0.15–0.52 μm^2) without significantly affecting the portion of axons with smaller or larger caliber (up to 1 μm^2) (Fig. 5C). This increase in size did not accompany an overall difference in the total number of axons because mean axon number did not differ between the minocycline-treated (33,548 ± 11,980 axons) and the vehicle-treated groups (38,428 ± 15,059 axons; $P = 0.31$). This was not unexpected. In a previous study, we demonstrated that in each age group, differences in IOP trans-

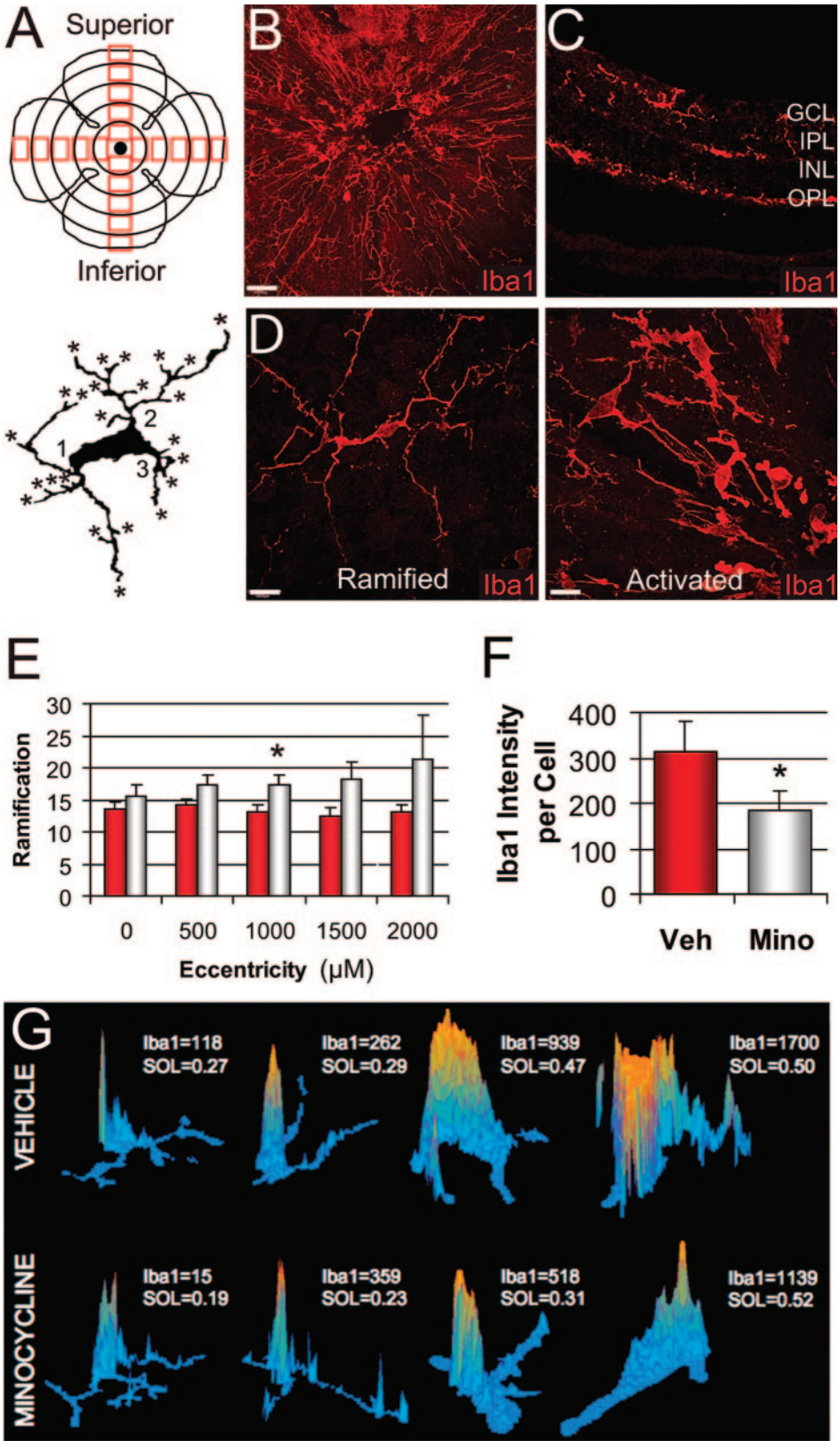

FIGURE 3. (**A**) *Boxes* arrayed on the retina schematic represent counting fields within each quadrant; the *circle* centered on the ONH is 1000 μm in diameter; *concentric circles* are spaced 500 μm apart and defining fields are binned (**E**). Ramification as a measure of shape complexity is the number of process tips divided by the number of primary processes in the microglial cell. The microglia silhouette has 24 tips (*asterisk*) and three primary processes (numbered 1-3), and the ramification is 8. (**B**) Image of the central 1000 μm in a retinal flatmount immunostained for Iba1 highlights the arrangement of microglia. Scale bar, 100 μm. (**C**) Radial section of a retina identically labeled identifies the three retinal depths at which microglial cells distribute: GCL, IPL, and OPL. Scale bar, 100 μm. (**D**) At high magnification, Iba1-labeled microglia show diverse morphologic complexity, from highly ramified (resting state) to round somata with sturdy and simplified processes (activated state). Scale bar, 10 μm. (**E**) Analysis of retinal microglial ramification at increasing eccentricity established greater numbers of highly ramified microglia in retinas from mice dosed for 25 weeks with minocycline (*light bars*) compared with vehicle-treated retinas (*dark bars*); statistically significant at mid-periphery (1000 μm; $^*P < 0.05$). Error bars = SEM. (**F**) Histogram of Iba1 immunofluorescence densitometry in individual microglial cells shows significantly decreased expression in minocycline-treated retinas ($^*P < 0.001$). Error bars = SEM. (**G**) Histograms of relative Iba1 intensity in microglia cells with diverse solidity (cell area divided by the area of the polygon bounded by the cell) show that morphologically matched microglia, with identical solidity values (*far right*), express higher Iba1 intensities in vehicle- than in minocycline-treated mice. These two microglial cells represent the peak values for Iba1 immunoexpression intensity found within both experimental groups among all cells measured.

late to differences in axon survival, so that each age group is represented by a large spread in axon number.[23] When plotted against mean IOP for each nerve, the vehicle-only group demonstrated the typical IOP-dependent loss of RGC axons, as indicated by the negative slope of the best-fitting regression line (Fig. 5E). This loss ranged from approximately 5000 to 10,000 axons for each 1-mm Hg increment in mean IOP, similar to the rate of loss we documented for comparably aged animals in our previous work.[23] However, in the minocycline-treated animals, we did not observe the expected loss of axons with

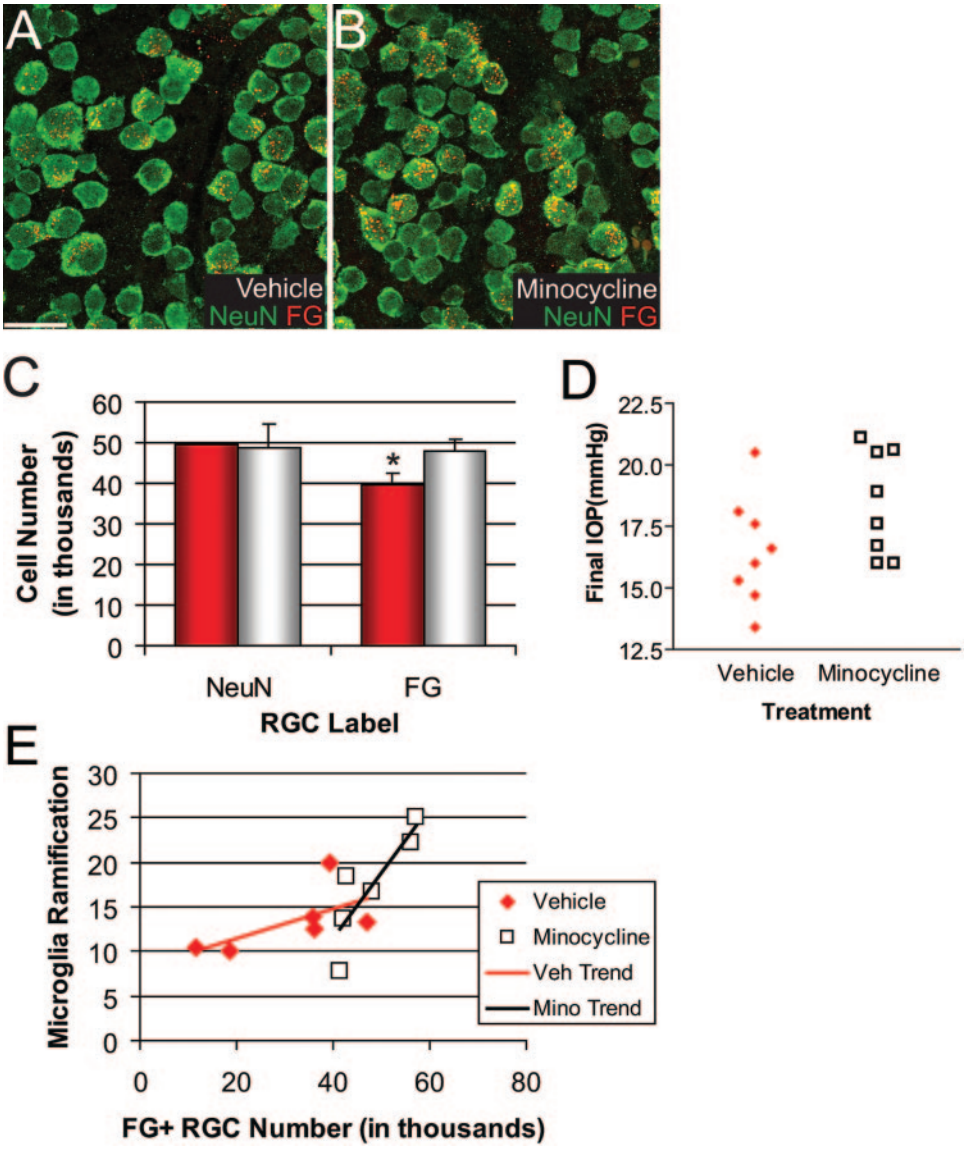

FIGURE 4. (**A**, **B**) Retinal flatmounts show NeuN-positive RGCs (*green*) and a RGC subset retrogradely labeled with neuronal retrograde tracer (*red*). Notice that neuronal retrograde tracer labeling is more intense and more abundant in more RGCs after minocycline treatment (**B**) than after vehicle treatment (**A**). Scale bar, 25 μm. (**C**) Quantitative stereology of NeuN-positive RGCs and neuronal retrograde tracer-positive RGCs in flatmounted retinas dosed with vehicle (*dark bars*, $n = 8$) or minocycline (*light bars*, $n = 7$) showed no differences in the total number of NeuN-positive RGCs per retina between treatments but significantly more retrogradely labeled neuronal retrograde tracer-positive RGCs in the minocycline-treated retinas ($^*P < 0.05$). Error bars = SEM. (**D**) Final IOP measures of vehicle- and minocycline-treated mice that underwent neuronal retrograde tracing did not differ, as shown by this scatter plot. (**E**) Scatter plot of microglia ramification (as measured 1000 μM from ONH) compared with the number of neuronal retrograde tracer-positive RGCs for the vehicle- and minocycline-treated groups shows that microglia ramification is more tightly correlated with neuronal retrograde tracer-positive cell number in the minocycline group ($r^2 = 0.73$) than in the vehicle treatment group ($r^2 = 0.39$).

increasing IOP, even for the highest IOPs (IOP >17 mm Hg). Analysis of covariance using indicator variables demonstrated that the best-fitting regression line for the minocycline group approached a slope of zero, indicating no dependence on IOP ($P = 55$), but that the difference between the slopes for the minocycline- versus vehicle-only group was highly significant ($P < 0.001$).

DISCUSSION

This study demonstrates that long-term and systemic treatment of DBA/2J mice with minocycline, commencing before clinical evidence of glaucoma, suppressed retinal microglial activation and improved ganglion cell integrity, supporting the hypothesis that retinal microglia may contribute to RGC pathology after IOP elevation.

Previous studies have shown microglial activation and redistribution in the human glaucomatous ONH[11,32] and in retinas under acute ocular hypertension.[41,42] It is known that microglia cells have extremely plastic morphology, transformable from finely ramified shapes during resting state to larger somata with a few broad processes and eventually to solid, globular phagocytes.[43,44] Moreover, activated microglia upregulate specific genes, such as Iba1, after axotomy,[33] ischemia,[45] and neural disorders.[46,47] We show that with long-term minocycline treatment, retinal microglia maintain a complex, ramified morphology, demonstrating a lack of activation. Here, minocycline also prevented retinal microglia from upregulating Iba1 mRNA and protein expression, confirming their reduced activation. Multiple reports demonstrate that minocycline can effectively suppress microglial activation in vivo and in vitro, preventing the production of inflammatory cytokines.[16,48,49] We found that the numbers of retinal microglia did not differ between the experimental groups, suggesting that although activation was reduced, minocycline did not affect the modest proliferation occurring in DBA/2J retinas,[20] as also seen in some injury models.[50]

Although minocycline can directly suppress cell death pathways[51] we observed comparable amounts of apoptotic RGCs between experimental groups, which suggests that apoptosis might not have been the primary mechanism of action of minocycline in our study. Consistent with this, RGC apoptosis is detectable but not significant at 6 months[40] and peaks in 10- to 13-month-old DBA/2J mice.[23] Other reported effects of minocycline, such as suppression of matrix metalloproteinase and[52] nitric oxide and free radical[48] production, might have

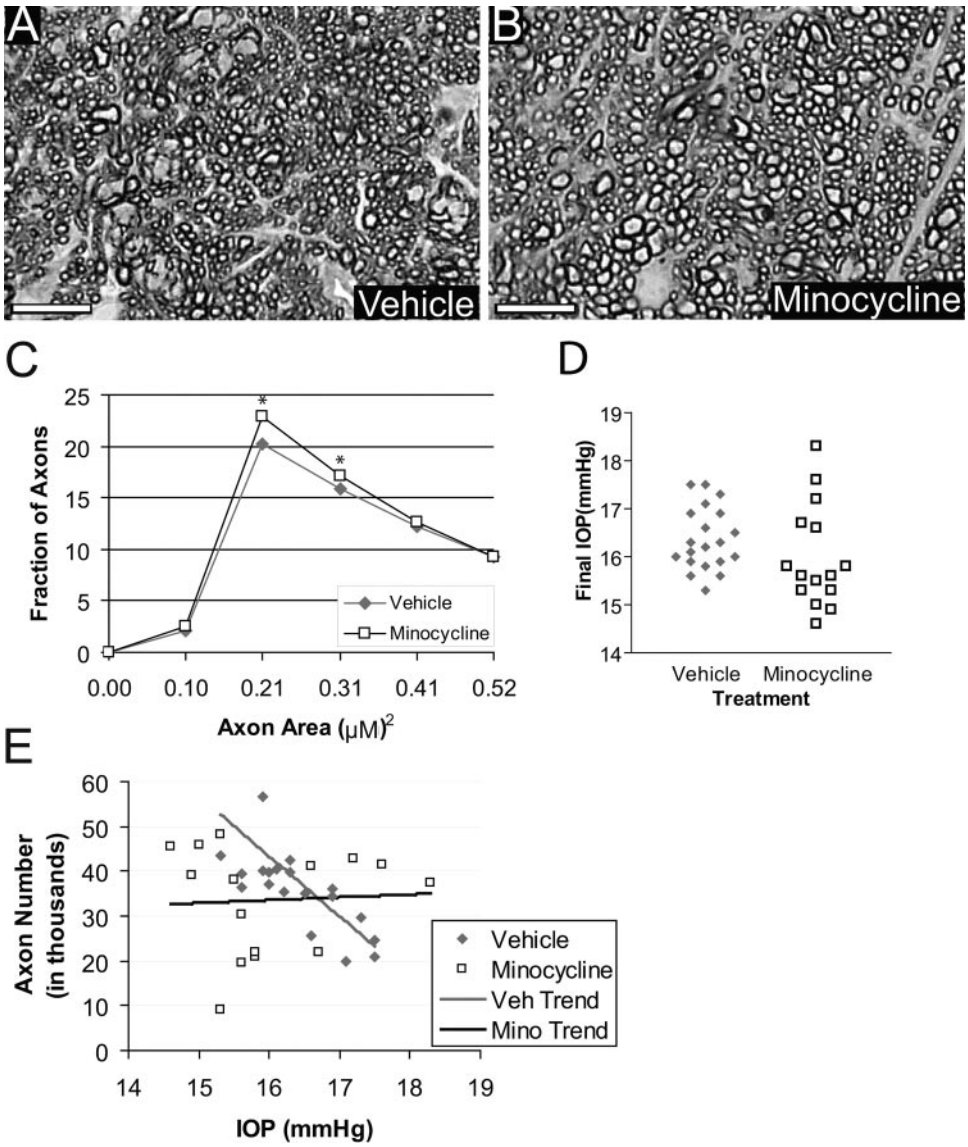

FIGURE 5. RGC axon cross-section in proximal optic nerve from 7-month-old mice. (**A**) Vehicle-treated mice with 17.5-mm Hg mean IOP had a mean axon density of 191,823 axons/mm^2 (21,000 total axons); note disorganization of fascicles and aberrations in myelin wraps (*arrows*). This was typical within our population of animals with comparable ages and IOP levels. Scale bar, 10 μm. (**B**) Minocycline-treated mouse with 17.6-mm Hg mean IOP showed a mean axon density of 317,175 axons/mm^2 (41,400 total axons) with more ordered fascicles and normal myelin wraps. Scale bar, 10 μm. (**C**) Histogram of axon area shows a different proportion of axons in bins 0.1 to 0.4 (μm^2) in the minocycline-compared with the vehicle-treated group. There was a significantly higher fraction of minocycline-treated RGC axons in the 0.21 and 0.31 (μm^2) bins ($^*P < 0.023$), but no difference in the proportions of vehicle- and minocycline-treated axons with diameters greater than 0.52 (μm^2) was detected (data not shown). (**D**) Scatter plot of mean IOP in mice whose optic nerves were analyzed shows no statistical difference between groups. (**E**) Scatter plot of axon number versus mean IOP illustrates that in vehicle-treated mice, higher IOP significantly ($P < 0.001$) correlated with lower RGC axon number in optic nerve, whereas this relationship was abolished with minocycline treatment. For the regression lines, $r^2 = 0.56$ (vehicle) and $r^2 = 0.003$ (minocycline).

contributed to the improved RGC retrograde labeling we observed, though in some cases these actions were likely secondary to reduced microglial activation.

Anterior segment pathology and IOP elevation were unchanged with minocycline treatment. Although minocycline has suppressive effects on inflammatory cells, such as T lymphocytes and monocytes,[52,53] the absence of inflammation and blood-barrier disruption in DBA/2J retina[40] suggests that these also are not targets of minocycline action.

Having previously demonstrated that the DBA/2J retina mounts a reactive gliosis, consisting of astrocytic and Müller glia hypertrophy,[20] we explored whether minocycline affects glial populations. Minocycline had no apparent effect on astrocyte numbers and hypertrophy or Müller gliosis, consistent with previous reports[16] showing no difference in the number of activated astrocytes, but significant reductions in microglia numbers did result after minocycline treatment of mice modeling cerebrovascular amyloid deposition. However, in an experimental autoimmune encephalomyelitis model of optic neuritis, minocycline affected Müller cells and astrocytes.[19] The nature of the central nervous system abnormality might have influenced the effect of minocycline on glia given that other studies have shown minocycline reducing astrocyte numbers and hypertrophy in models of spinal cord injury[54] and Huntington disease.[55] Although our findings argue that gliosis is not sufficient to drive RGC pathology, retinal glia alter their microenvironment, potentially contributing to glaucoma.[15,56–60] Further studies will be needed to determine how interaction between RGCs, microglia, Müller cells, and astrocytes influence glaucoma progression.

Several different measures suggested a protective effect of minocycline treatment on RGC viability. Long-term minocycline treatment uncoupled the relationship between IOP elevation and declining axon density typical in DBA/2J optic nerves[21] without changing the overall optic nerve axon density. Minocycline also promoted greater numbers of mid-caliber axons, and, because our axon area measurements excluded myelin wraps, increases in axon area most likely indicated increased content of structural proteins, suggesting a reversal in the progression toward axon degeneration normally observed in aging DBA/2J mice. Our observation of phosphorylated heavy chain neurofilament accumulation in RGC somata and proximal axons of severely affected DBA/2J retinas can indicate transport failure through declining axons.[61] Minocycline may affect neurofilament and microtubule deposition directly by improving transport of these cargoes. Alternatively, it may maintain the expression of structural proteins because retinas from severely affected DBA/2J mice show significant

downregulation of neurofilament expression (Buckingham BP, et al., manuscript submitted), indicative of changes in axon caliber.[62] In development, structural proteins increase in myelinated nerve regions,[63] and there is evidence that activated microglia can influence oligodendrocytes, myelination, or both.[64] Microglia may contribute to axon decline, as evidenced by microglia promoting the breakdown of axonal transport of synaptic precursors[65] and neuritic beading preceding neuronal death,[66] demonstrating a relationship with axonal integrity. Consistent with this, minocycline increased the number of retrogradely labeled RGCs while it reduced the activation state of retinal microglia, suggesting an improvement in axon transport function or connectivity to the central target.

Our findings are consistent with those of previous studies showing that minocycline improves RGC viability after axotomy,[17] ocular hypertension,[67] and experimental autoimmune encephalomyelitis optic neuritis.[19] The underlying selective reduction of microglial activation points to a contribution for these neuroinflammatory cells to DBA/2J glaucoma, without excluding a role for other components. The fact that minocycline is protective in DBA/2J mice suggests that glaucoma may share overlapping cellular or molecular mechanisms with classic neurodegenerative diseases, which proved minocycline neuroprotective actions in animal models[24,51–57,59–66,69] and has led to the testing of minocycline therapeutic efficacy in several human trials.[70] Future studies will determine whether features of glaucoma are shared with other neurodegenerative diseases.

Acknowledgments

The authors thank Holly M. Nguyen for mouse gavage and IOP measurement.

References

1. Ahmed F, Brown KM, Stephan DA, Morrison JC, Johnson EC, Tomarev SI. Microarray analysis of changes in mRNA levels in the rat retina after experimental elevation of intraocular pressure. *Invest Ophthalmol Vis Sci*. 2004;45:1247–1258.
2. Johnson EC, Jia L, Cepurna WO, Doser TA, Morrison JC. Global changes in optic nerve head gene expression after exposure to elevated intraocular pressure in a rat glaucoma model. *Invest Ophthalmol Vis Sci*. 2007;48:3161–3177.
3. Miyahara T, Kikuchi T, Akimoto M, Kurokawa T, Shibuki H, Yoshimura N. Gene microarray analysis of experimental glaucomatous retina from cynomologus monkey. *Invest Ophthalmol Vis Sci*. 2003;44:4347–4356.
4. Naskar R, Thanos S. Retinal gene profiling in a hereditary rodent model of elevated intraocular pressure. *Mol Vis*. 2006;12:1199–1210.
5. Steele MR, Inman DM, Calkins DJ, Horner PJ, Vetter ML. Microarray analysis of retinal gene expression in the DBA/2J model of glaucoma. *Invest Ophthalmol Vis Sci*. 2006;47:977–985.
6. Langmann T. Microglia activation in retinal degeneration. *J Leukoc Biol*. 2007;81:1345–1351.
7. Thanos S. The relationship of microglial cells to dying neurons during natural neuronal cell death and axotomy-induced degeneration of the rat retina. *Eur J Neurosci*. 1991;3:1189–1207.
8. Chauhan BC, Pan J, Archibald ML, LeVatte TL, Kelly ME, Tremblay F. Effect of intraocular pressure on optic disc topography, electroretinography, and axonal loss in a chronic pressure-induced rat model of optic nerve damage. *Invest Ophthalmol Vis Sci*. 2002;43:2969–2976.
9. Hughes EH, Schlichtenbrede FC, Murphy CC, et al. Generation of activated sialoadhesin-positive microglia during retinal degeneration. *Invest Ophthalmol Vis Sci*. 2003;44:2229–2234.
10. Chauhan BC, LeVatte TL, Jollimore CA, et al. Model of endothelin-1-induced chronic optic neuropathy in rat. *Invest Ophthalmol Vis Sci*. 2004;45:144–152.
11. Neufeld AH. Microglia in the optic nerve head and the region of parapapillary chorioretinal atrophy in glaucoma. *Arch Ophthalmol*. 1999;117:1050–1056.
12. Tezel G, Chauhan BC, LeBlanc RP, Wax MB. Immunohistochemical assessment of the glial mitogen-activated protein kinase activation in glaucoma. *Invest Ophthalmol Vis Sci*. 2003;44:3025–3033.
13. Block ML, Zecca L, Hong JS. Microglia-mediated neurotoxicity: uncovering the molecular mechanisms. *Nat Rev Neurosci*. 2007;8:57–69.
14. Kim SU, de Vellis J. Microglia in health and disease. *J Neurosci Res*. 2005;81:302–313.
15. Tezel G, Wax MB. Glaucoma. *Chem Immunol Allergy*. 2007;92:221–227.
16. Fan R, Xu F, Previti ML, et al. Minocycline reduces microglial activation and improves behavioral deficits in a transgenic model of cerebral microvascular amyloid. *J Neurosci*. 2007;27:3057–3063.
17. Baptiste DC, Powell KJ, Jollimore CA, et al. Effects of minocycline and tetracycline on retinal ganglion cell survival after axotomy. *Neuroscience*. 2005;134:575–582.
18. Levkovitch-Verbin H, Quigley HA, Martin KR, et al. The transcription factor c-jun is activated in retinal ganglion cells in experimental rat glaucoma. *Exp Eye Res*. 2005;80:663–670.
19. Maier K, Merkler D, Gerber J, et al. Multiple neuroprotective mechanisms of minocycline in autoimmune CNS inflammation. *Neurobiol Dis*. 2007;25:514–525.
20. Inman DM, Horner PJ. Reactive non-proliferative gliosis predominates in a chronic mouse model of glaucoma. *Glia*. 2007;55:942–953.
21. Inman DM, Sappington RM, Horner PJ, Calkins DJ. Quantitative correlation of optic nerve pathology with ocular pressure and corneal thickness in the DBA/2 mouse model of glaucoma. *Invest Ophthalmol Vis Sci*. 2006;47:986–996.
22. John SW, Smith RS, Savinova OV, et al. Essential iris atrophy, pigment dispersion, and glaucoma in DBA/2J mice. *Invest Ophthalmol Vis Sci*. 1998;39:951–962.
23. Libby RT, Anderson MG, Pang IH, et al. Inherited glaucoma in DBA/2J mice: pertinent disease features for studying the neurodegeneration. *Vis Neurosci*. 2005;22:637–648.
24. Du Y, Ma Z, Lin S, et al. Minocycline prevents nigrostriatal dopaminergic neurodegeneration in the MPTP model of Parkinson's disease. *Proc Natl Acad Sci U S A*. 2001;98:14669–14674.
25. Hill GB. Therapeutic evaluation of minocycline and tetracycline for mixed anaerobic infection in mice. *Antimicrobial Agents Chemother*. 1977;11:625–630.
26. Bosco A, Cusato K, Nicchia GP, Frigeri A, Spray DC. A developmental switch in the expression of aquaporin-4 and Kir4.1 from horizontal to Muller cells in mouse retina. *Invest Ophthalmol Vis Sci*. 2005;46:3869–3875.
27. Colovic M, Caccia S. Liquid chromatographic determination of minocycline in brain-to-plasma distribution studies in the rat. *J Chromatogr*. 2003;791:337–343.
28. Fuller JL, Sjursen FH Jr. Audiogenic seizures in eleven mouse strains. *J Hered*. 1967;58:135–140.
29. Mo JS, Anderson MG, Gregory M, et al. By altering ocular immune privilege, bone marrow-derived cells pathogenically contribute to DBA/2J pigmentary glaucoma. *J Exp Med*. 2003;197:1335–1344.
30. Zhou X, Li F, Kong L, Tomita H, Li C, Cao W. Involvement of inflammation, degradation, and apoptosis in a mouse model of glaucoma. *J Biol Chem*. 2005;280:31240–31248.
31. Imai Y, Ibata I, Ito D, Ohsawa K, Kohsaka S. A novel gene Iba1 in the major histocompatibility complex class III region encoding an EF hand protein expressed in a monocytic lineage. *Biochem Biophys Res Commun*. 1996;224:855–862.
32. Yuan L, Neufeld AH. Activated microglia in the human glaucomatous optic nerve head. *J Neurosci Res*. 2001;64:523–532.
33. Ito D, Imai Y, Ohsawa K, Nakajima K, Fukuuchi Y, Kohsaka S. Microglia-specific localisation of a novel calcium binding protein, Iba1. *Brain Res Mol Brain Res*. 1998;57:1–9.
34. Sasaki Y, Ohsawa K, Kanazawa H, Kohsaka S, Imai Y. Iba1 is an actin-cross-linking protein in macrophages/microglia. *Biochem Biophys Res Commun*. 2001;286:292–297.

35. Ohsawa K, Imai Y, Kanazawa H, Sasaki Y, Kohsaka S. Involvement of Iba1 in membrane ruffling and phagocytosis of macrophages/microglia. *J Cell Sci*. 2000;113(pt 17):3073–3084.
36. Canola K, Angenieux B, Tekaya M, et al. Retinal stem cells transplanted into models of late stages of retinitis pigmentosa preferentially adopt a glial or a retinal ganglion cell fate. *Invest Ophthalmol Vis Sci*. 2007;48:446–454.
37. Dijk F, Bergen AA, Kamphuis W. GAP-43 expression is upregulated in retinal ganglion cells after ischemia/reperfusion-induced damage. *Exp Eye Res*. 2007;84:858–867.
38. Zhong L, Bradley J, Schubert W, et al. Erythropoietin promotes survival of retinal ganglion cells in DBA/2J glaucoma mice. *Invest Ophthalmol Vis Sci*. 2007;48:1212–1218.
39. Zhu S, Stavrovskaya IG, Drozda M, et al. Minocycline inhibits cytochrome *c* release and delays progression of amyotrophic lateral sclerosis in mice. *Nature*. 2002;417:74–78.
40. Schuettauf F, Rejdak R, Walski M, et al. Retinal neurodegeneration in the DBA/2J mouse-a model for ocular hypertension. *Acta Neuropathol (Berl)*. 2004;107:352–358.
41. Wang X, Tay SS, Ng YK. An immunohistochemical study of neuronal and glial cell reactions in retinae of rats with experimental glaucoma. *Exp Brain Res*. 2000;132:476–484.
42. Naskar R, Wissing M, Thanos S. Detection of early neuron degeneration and accompanying microglial responses in the retina of a rat model of glaucoma. *Invest Ophthalmol Vis Sci*. 2002;43:2962–2968.
43. Banati RB. Neuropathological imaging: in vivo detection of glial activation as a measure of disease and adaptive change in the brain. *Br Med Bull*. 2003;65:121–131.
44. Kreutzberg GW. Microglia: a sensor for pathological events in the CNS. *Trends Neurosci*. 1996;19:312–318.
45. Ito D, Tanaka K, Suzuki S, Dembo T, Fukuuchi Y. Enhanced expression of Iba1, ionized calcium-binding adapter molecule 1, after transient focal cerebral ischemia in rat brain. *Stroke J Cereb Circ*. 2001;32:1208–1215.
46. Mori I, Imai Y, Kohsaka S, Kimura Y. Upregulated expression of Iba1 molecules in the central nervous system of mice in response to neurovirulent influenza A virus infection. *Microbiol Immunol*. 2000;44:729–735.
47. von Eitzen U, Egensperger R, Kosel S, et al. Microglia and the development of spongiform change in Creutzfeldt-Jakob disease. *J Neuropathol Exp Neurol*. 1998;57:246–256.
48. Wang AL, Yu AC, Lau LT, et al. Minocycline inhibits LPS-induced retinal microglia activation. *Neurochem Int*. 2005;47:152–158.
49. Yrjanheikki J, Tikka T, Keinanen R, Goldsteins G, Chan PH, Koistinaho J. A tetracycline derivative, minocycline, reduces inflammation and protects against focal cerebral ischemia with a wide therapeutic window. *Proc Natl Acad Sci U S A*. 1999;96:13496–13500.
50. Fendrick SE, Miller KR, Streit WJ. Minocycline does not inhibit microglia proliferation or neuronal regeneration in the facial nucleus following crush injury. *Neurosci Lett*. 2005;385:220–223.
51. Wang X, Zhu S, Drozda M, et al. Minocycline inhibits caspase-independent and -dependent mitochondrial cell death pathways in models of Huntington's disease. *Proc Natl Acad Sci U S A*. 2003;100:10483–10487.
52. Brundula V, Rewcastle NB, Metz LM, Bernard CC, Yong VW. Targeting leukocyte MMPs and transmigration: minocycline as a potential therapy for multiple sclerosis. *Brain*. 2002;125:1297–1308.
53. Kloppenburg M, Brinkman BM, de Rooij-Dijk HH, et al. The tetracycline derivative minocycline differentially affects cytokine production by monocytes and T lymphocytes. *Antimicrobial Agents Chemother*. 1996;40:934–940.
54. Teng YD, Choi H, Onario RC, et al. Minocycline inhibits contusion-triggered mitochondrial cytochrome c release and mitigates functional deficits after spinal cord injury. *Proc Natl Acad Sci U S A*. 2004;101:3071–3076.
55. Ryu JK, Choi HB, McLarnon JG. Combined minocycline plus pyruvate treatment enhances effects of each agent to inhibit inflammation, oxidative damage, and neuronal loss in an excitotoxic animal model of Huntington's disease. *Neuroscience*. 2006;141:1835–1848.
56. Fu QL, Wu W, Wang H, Li X, Lee VW, So KF. Up-regulated endogenous erythropoietin/erythropoietin receptor system and exogenous erythropoietin rescue retinal ganglion cells after chronic ocular hypertension. *Cell Mol Neurobiol*. In press.
57. Grieshaber MC, Terhorst T, Flammer J. The pathogenesis of optic disc splinter haemorrhages: a new hypothesis. *Acta Ophthalmol Scand*. 2006;84:62–68.
58. Liu B, Johns TG, Neufeld AH. Epidermal growth factor receptor activation: an upstream signal for transition of quiescent astrocytes into reactive astrocytes after neural injury. *J Neurosci*. 2006;26:7532–7540.
59. Malone PE, Hernandez MR. 4-Hydroxynonenal, a product of oxidative stress, leads to an antioxidant response in optic nerve head astrocytes. *Exp Eye Res*. 2007;84:444–454.
60. Woldemussie E, Wijono M, Ruiz G. Muller cell response to laser-induced increase in intraocular pressure in rats. *Glia*. 2004;47:109–119.
61. Soto I, Oglesby E, Buckingham BP, et al. Retinal ganglion cells downregulate gene expression and lose their axons within the optic nerve head in a mouse glaucoma model. *J. Neurosci.* 2008;28:548–561.
62. Hoffman PN, Cleveland DW, Griffin JW, Landes PW, Cowan NJ, Price DL. Neurofilament gene expression: a major determinant of axonal caliber. *Proc Natl Acad Sci U S A*. 1987;84:3472–3476.
63. Sanchez I, Hassinger L, Paskevich PA, Shine HD, Nixon RA. Oligodendroglia regulate the regional expansion of axon caliber and local accumulation of neurofilaments during development independently of myelin formation. *J Neurosci*. 1996;16:5095–5105.
64. Nakazawa T, Nakazawa C, Matsubara A, et al. Tumor necrosis factor-alpha mediates oligodendrocyte death and delayed retinal ganglion cell loss in a mouse model of glaucoma. *J Neurosci*. 2006;26:12633–12641.
65. Stagi M, Dittrich PS, Frank N, Iliev AI, Schwille P, Neumann H. Breakdown of axonal synaptic vesicle precursor transport by microglial nitric oxide. *J Neurosci*. 2005;25:352–362.
66. Takeuchi H, Mizuno T, Zhang G, et al. Neuritic beading induced by activated microglia is an early feature of neuronal dysfunction toward neuronal death by inhibition of mitochondrial respiration and axonal transport. *J Biol Chem*. 2005;280:10444–10454.
67. Levkovitch-Verbin H, Kalev-Landoy M, Habot-Wilner Z, Melamed S. Minocycline delays death of retinal ganglion cells in experimental glaucoma and after optic nerve transection. *Arch Ophthalmol*. 2006;124:520–526.
68. Zhao C, Ling Z, Newman MB, Bhatia A, Carvey PM. TNF-alpha knockout and minocycline treatment attenuates blood-brain barrier leakage in MPTP-treated mice. *Neurobiol Dis*. 2007;26:36–46.
69. Yong VW, Giuliani F, Xue M, Bar-Or A, Metz LM. Experimental models of neuroprotection relevant to multiple sclerosis. *Neurology*. 2007;68:S32–S37; discussion S43–S54.
70. Traynor BJ, Bruijn L, Conwit R, et al. Neuroprotective agents for clinical trials in ALS: a systematic assessment. *Neurology*. 2006;67:20–27.